Local structure and electronic state of a photomagnetic material of CoW cyanide studied by x-ray-absorption fine structure spectroscopy

Toshihiko Yokoyama,* Kaoru Okamoto, and Toshiaki Ohta
Department of Chemistry, Graduate School of Science, The University of Tokyo, 7-3-1 Hongo, Bunkyo-ku, Tokyo 113-0033, Japan

Shin-ichi Ohkoshi and Kazuhito Hashimoto
Research Center for Advanced Science and Technology, The University of Tokyo, 4-6-1 Komaba, Meguro-ku, Tokyo 153-0041, Japan
(Received 5 June 2001; revised manuscript received 14 August 2001; published 23 January 2002)

The local structure and electronic state of a photomagnetic material $Cs_{0.8}Co_{1.1}(3\text{-cyanopyridine})_{1.9}W(CN)_8 \cdot 2.1H_2O$ have been investigated by means of x-ray-absorption fine structure (XAFS) spectroscopy. The Co *K*- and W *L*-edge x-ray-absorption near-edge structure has clarified that upon the transition from the high-temperature (HT) phase to the low-temperature (LT) one, a Co $3d$ electron is transferred to the W $5d$ level; the electronic state of Co changes from the high-spin divalent state (d^7, spin momentum $S=3/2$) to the low-spin trivalent state ($d^6, S=0$), while the W state correspondingly varies from the pentavalent state ($d^1, S=1/2$) to the tetravalent one ($d^2, S=0$). Extended XAFS analysis has revealed that the coordination around W and Co is $W(CN)_8Co_4$ and $Co(NC)_4(3\text{-cyanopyridine})_2W_4$, respectively, and that the Co-N distance in the LT phase is decreased by ~ 0.17 Å compared to that in the HT one, while the structure around W shows little change. We have also found x-ray-induced phase transition of the present material at 30 K. The x-ray-induced phase was found to be structurally and electronically identical to the HT phase.

DOI: 10.1103/PhysRevB.65.064438 PACS number(s): 75.30.Kz, 61.10.Ht, 75.50.−y, 75.50.Gg

I. INTRODUCTION

Prussian blue analogs have recently attracted great interest because of their noble magnetic properties. Sato *et al.*[1] discovered the phase transition in CoFe cyanides by optical stimuli; $Na_{0.4}Co_{1.3}Fe(CN)_6$ and $K_{0.4}Co_{1.3}Fe(CN)_6$ show weak paramagnetism at low temperature (LT), and they become ferrimagnets upon visible-light (500–750 nm) irradiation. The ferrimagnetic behavior is preserved up to ~ 100 K. Moreover, irradiation of near-infrared light (1319 nm) transforms the ferrimagnetic phase to the LT phase with weak paramagnetism. In our previous studies,[2,3] the local structure and the electronic properties of these CoFe cyanides were investigated by means of Fe and Co *K*-edge x-ray-absorption fine structure (XAFS) spectroscopy. It was revealed that during the spin transition from the high-temperature (HT) phase to the LT phase, the Co-N distance is compressed by 0.20 Å, associated with the change of the electronic states from Fe(III)LS ($S=1/2$) and Co(II)HS ($S=3/2$) of the HT phase to Fe(II)LS ($S=0$) and Co(III)LS ($S=0$) of the LT phase. Here, LS and HS imply low spin and high spin, respectively, and *S* is the spin angular momentum. The photomagnetized phase at 30 K was found to be structurally and electronically identical to the HT phase. Cartier dit Moulin *et al.*[4] independently investigated the Fe and Co *K*-edge XAFS of a similar CoFe cyanide $Rb_{0.5}Co_{1.3}[Fe(CN)_6] \cdot 3.9H_2O$, and their results are consistent with our findings. Moreover, they examined Fe and Co *L*-edge x-ray-absorption near-edge structure (XANES) and obtained further detailed information on the electronic states.

Very recently, Hashimoto *et al.*[5] found similar photomagnetization in a new type of transition metal cyanide. The chemical formula of this material is $Cs_{0.8}Co_{1.1}W(CN)_8(3\text{-CNpy})_{1.9} \cdot 2.1H_2O$(3-CNpy = 3-cyanopyridine). Apparently, the structure of the salt is not a simple rock salt structure as in the CoFe cyanides, because the W atom is coordinated by eight CN^- ligands. It was suggested from susceptibility measurements that the CoW cyanide is paramagnetic at room temperature [d^7HS($S=3/2$) for Co and d^1($S=1/2$) for W are expected] and undergoes a first-order spin transition at $T_{\downarrow c}=152$ K (cooling process) and $T_{\uparrow c}=206$ K (warming). The LT phase shows very weak paramagnetism, thus indicating that the charge-transfer transition occurs and the electronic state of Co changes from Co(II)HS to Co(III)LS. On visible-light irradiation below 30 K, however, the material shows ferrimagnetism. Although the HT phase does not show spontaneous magnetization at room temperature because of the lack of three-dimensional magnetic ordering, the local electronic state of the trapped excited state at low temperature may be similar to the HT phase.

In order to understand these magnetic properties in detail, structural information is indispensable. It is, however, essentially difficult to obtain single crystals for x-ray crystallography as is often the case of Prussian blue analogs. XAFS spectroscopy is thus suitable to determine the structure of CoW cyanide. In the present study, we have investigated the electronic and local atomic structures of the HT and LT phases of the CoW cyanide by means of Co *K*- and W *L*-edge XAFS spectroscopy. Moreover, we have found an x-ray-induced phase transition at 30 K as in the case of visible-light irradiation. The structure and electronic properties of the phase have also been examined. It is also demonstrated that high-resolution W *L*-edge XANES measurements allow us to distinguish pentavalent W from tetravalent, this being a key issue to identify the charge-transfer spin transition in the present material.

This article is organized as follows. In Sec. II, experimental details are given for spectroscopic measurements. Section III deals with results and discussion. In Sec. III A, we show time evolution of the Co *K*-edge XANES during x-ray irradiation at 30 K. In Sec. III B, Co *K*- and W *L*-edge XANES, the electronic states of Co and W, are described. In Sec. III C, the analysis results of Co *K*- and W L_{III}-edge extended x-ray-absorption fine structure (EXAFS) are given. Section IV gives a summary of the present investigation.

II. EXPERIMENTS

$Cs_{0.8}Co_{1.1}W(CN)_8$(3-cyanopyridine)$_{1.9}\cdot 2.1H_2O$ was prepared according to the previous work.[5] Co *K*- and W *L*-edge XAFS spectra of CoW cyanide were taken in the conventional transmission mode at Beamlines 10B and 12C of the Photon Factory (operation energy of 2.5 GeV and stored current of 400–250 mA) in the Institute of Materials Structure Science (KEK-PF). At Beamline 10B, a Si(311) channel-cut crystal (the first crystal was cooled with water) was employed as the monochromator. The photon density was of the order of 10^8 photons/s/mm^2 and the spot size was 5×1 mm^2. The effect of higher-order harmonics was not so important at Beamline 10 B for the measurements of Co *K* and W *L* edges under 2.5 GeV operation when the total absorption coefficient was less than ~ 4. At Beamline 12C, a Si(111) double-crystal monochromator was installed. A set of focusing mirrors eliminated higher-order harmonics and the double crystals were detuned by $\sim 40\%$. The photon density was $\sim 10^{11}$ photons/s/mm^2 and the spot size was 1×1 mm^2. The intensities of the incident and transmitted x rays were recorded using ionization chambers filled with N_2. The sample was diluted with BN and pressed to prepare a disk (diameter of 13 mm). The total absorption coefficient was less than 3.0 and the edge jumps were ~ 0.3 for both Co *K* and W L_{III} edges. We also note that in the W $L_{III,II}$-edge XANES measurements, a shoulder structure was successfully detected only by using an Si(311) monochromator at Beamline 10B, while it could not be observed at focused Beamline 12C where an Si(111) monochromator was employed. This is presumably because of higher energy resolution of the monochromator at Beamline 10B.

Temperature-dependent XAFS measurements were performed at Beamline 10B. The samples investigated are listed in Table I. The HT phase was first examined at 300 K [sample (a)]. At low temperature, four samples with different HT/LT ratios were prepared depending on the rate of cooling [samples (b)–(e)]. The cooling rate followed the order of (b)>(c)>(d) [(b) ~ 0.2 K/s, (c) ~ 0.05 K/s, and (d) ~ 0.01 K/s], while the temperature of sample (e) was kept slightly below the transition temperature (130 K) for a couple of hours. The spectra of samples (b)–(d) were taken at 30 K, while those of sample (e) were measured at 130 K. For references, we also measured the W *L*-edge XAFS spectra of $Cs_3W^V(CN)_8\cdot 2H_2O$ [sample (R1)], $K_4W^{IV}(CN)_8\cdot 2H_2O$ [sample (R2)], and $Co_2W^{IV}(CN)_8\cdot zH_2O$ [sample (R3)] at 30 K. Typical data acquisition time was 1 s/point for XANES and 2–4 s/point for EXAFS.

At Beamline 12C, x-ray-induced phase transformation was examined at 30 K. For this purpose, the LT phase was at first prepared at 130 K in a manner similar to that of sample (e) and was cooled down to 30 K. During continuous Co *K*-edge XANES measurements (one XANES run took 54 s) the transformation was clearly observed. After x-ray irradiation at 30 K for 2 h the transformation was almost saturated, and the Co *K*- and W *L*-edge XAFS spectra were subsequently recorded [sample (f)]. Since the x rays at Beamline 12C were a few hundred times brighter than those at Beamline 10B, the absence of detectable changes observed at Beamline 10B during XAFS measurements was reasonable.

TABLE I. List of samples investigated. The composition ratio of Co^{II} is also given, which is obtained by the Co *K*-edge XANES analysis. Samples (R1), (R2), and (R3) are the reference samples, while samples (a)–(f) are the CoW cyanides of interest.

Sample	T (K)	Co^{II} ratio	Remarks
(R1)	30		$Cs_3W^V(CN)_8\cdot 2H_2O$
(R2)	30		$K_4W^V(CN)_8\cdot 2H_2O$
(R3)	30		$Co_2W^V(CN)_8\cdot 2H_2O$
(a)	300	98.9%	HT phase
(b)	30	85.0%	high cooling rate
(c)	30	69.3%	medium cooling rate
(d)	30	44.7%	low cooling rate
(e)	130	30.1%	T kept at 130 K
(f)	30	82.0%	x-ray irradiated

[a]Temperature for XAFS measurements.
[b]For an estimation of the Co^{II} ratio, see Sec. III B and Fig. 3 below.

III. RESULTS AND DISCUSSION

A. X-ray-induced phase transformation

Figure 1 shows the time evolution of the Co *K*-edge XANES spectra of CoW cyanide at 30 K during x-ray irradiation. At $t=0$, the spectrum exhibits a main peak at ~ 7723 eV. This clearly changes as the measurement proceeds; namely, the peak at ~ 7720 eV increases while the 7723 eV peak diminishes gradually. According to our previous works on CoFe cyanides,[2,3] the peaks at 7720 and 7723 eV can be attributed to Co(II)HS and Co(III)LS components, respectively. The peak shift between Co(II)HS and Co(III)LS ones mainly originates from considerable difference in Co-N distance, as discussed below in the EXAFS section. The resonance energy is likely to become higher as the bond distance becomes shorter.[6] It is therefore concluded that the CoW cyanide exhibits the x-ray-induced phase transition from the Co(III)LS state (LT phase) to the Co(II)HS state, as in the case of visible-light irradiation.[5]

In our previous CoFe studies,[2,3] we successfully determined the composition ratios of Co(II) and Co(III) quantitatively by employing the factor analysis technique.[7] When one gathers a lot of data sets consisting of a mixture of several spectral components, factor analysis allows one to determine the composition ratio of the components in each spectrum as well as the spectrum of each component. The optimization is carried out so that the square of the covari-

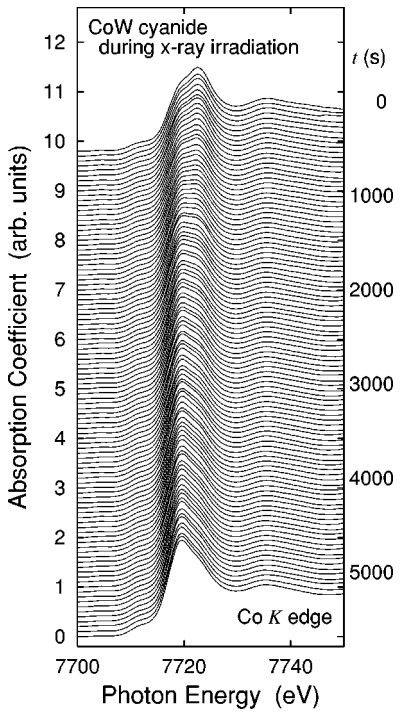

FIG. 1. Time evolution of the Co *K*-edge XANES spectra of CoW cyanide at 30 K during x-ray irradiation.

ance matrix gives the maximum (statistically most probable). Although the factor analysis often contains large ambiguities, the present case is quite simple because of the following reasons. First, the number of components is only 2 and the spectrum of the HT phase is almost known [spectrum (a) in Fig. 3; see below]. Moreover, the number of data sets is more than 100 as seen in Figs. 1 and 3, and this is sufficient to reduce statistical ambiguities. In the present case, the third largest eigenvalue of the covariance matrix is more than 200 times smaller than the second largest eigenvalue, implying that the third component in the data sets can be neglected with high reliability. The obtained logarithmic ratio, $\ln\{[Co^{III}]/([Co^{II}]+[Co^{III}])\}$, is plotted in Fig. 2. In the first-order phase transition, an abrupt change of the composition ratio should be observed, and this is not the present case. This may be because the present material consists of fine

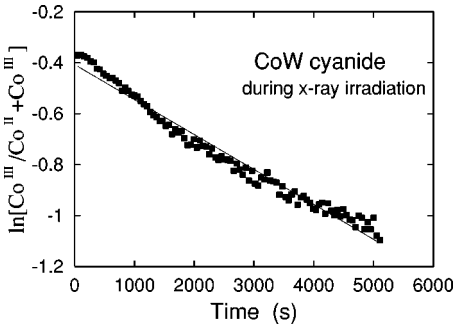

FIG. 2. Logarithmic ratio of the Co(III) component, $\ln\{[Co^{III}]/([Co^{II}]+[Co^{III}])\}$, as a function of time evaluated from Fig. 1 by employing the factor analysis (Ref. 7). The straight line corresponds to the first-order kinetics.

particles, each of which shows different behavior. On the other hand, the straight line in Fig. 2 corresponds to the the first-order kinetics of the transformation. One can find a slight curvature that indicates the presence of some particles that do not undergo the spin transition. Although the detailed mechanism of the phase transition cannot be discussed from the present results, the important conclusion here is that the x-ray-induced phase transition (or transformation) of CoW cyanide is definitely observed.

B. Co *K*- and W *L*-edge XANES

Figure 3 shows the Co *K*-edge XANES spectra of samples (a)–(f). Sample (a) exhibits a main peak at ~7720 eV, implying that Co is in the divalent HS state at 300 K. The spectrum of sample (b) taken at 30 K is, however, almost identical with that of sample (a). This indicates that rapid cooling allows the sample to preserve the (trapped) HT phase even at very low temperature. The spectra of samples (c) and (d) clearly show the peak at ~7723 eV, which is derived from Co(III)LS. Slower cooling facilitates the phase transition from HS to LS. Sample (e) gives the minimum ratio of Co(II)HS, the temperature being held at 130 K (slightly below $T_{\downarrow c}=152$ K). As already described above in Sec. III A, sample (f), which is irradiated by intense x rays, shows a spectrum similar to those of samples (a) and (b). This implies that the trapped excited phase induced by x rays consists of Co(II)HS, which may contribute to the ferrimagnetic behavior as in the visible-light irradiation. The

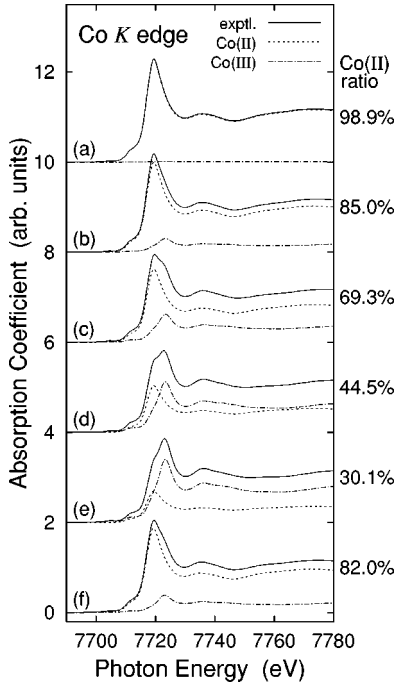

FIG. 3. Experimental Co *K*-edge XANES spectra (solid line) of samples (a)–(f). The spectra of Co(II) and Co(III) components obtained by factor analysis are given by dotted and dot-dashed lines, respectively, which are normalized according to their fractional contribution to the experimental spectra. The numerical values of the Co(II) ratio are also given.

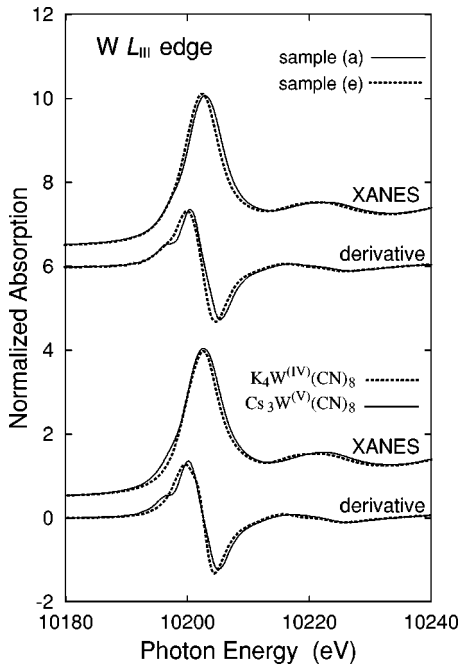

FIG. 4. W L_{III}-edge XANES spectra and their first derivatives for samples (a) (solid line, upper level) and (e) (dashed line, upper level). The reference spectra and their first derivatives (lower level) of sample (R1), $Cs_3W^V(CN)_8 \cdot 2H_2O$ (solid line), and sample (R2), $K_4W^{IV}(CN)_8 \cdot 2H_2O$ (dashed line), are also shown for comparison.

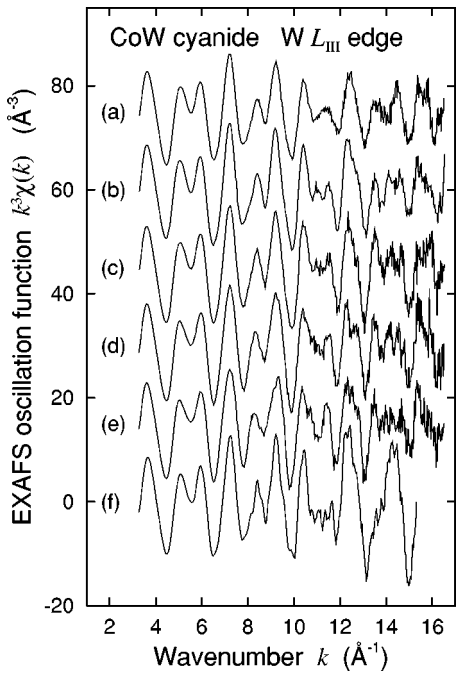

FIG. 5. W L_{III}-edge EXAFS oscillation function $k^3\chi(k)$ of samples (a)–(f). The temperatures of the measurements are 300 K for sample (a), 30 K for samples (b)–(d) and (f), and 130 K for sample (e).

local environment of sample (f) should be equivalent to the HT phase, although long-range magnetic order cannot be expected at higher temperatures. The results of the factor analysis are given in Fig. 3. The numerical values of the Co(II)HS ratios are important to analyze the EXAFS spectra discussed below.

Let us now focus on the W L-edge XANES. Figure 4 shows the W L_{III}-edge XANES spectra of samples (a) and (e), together with the reference spectra. W L_{II}-edge XANES gives almost identical results and are therefore omitted here. The peak height of the white line is almost the same among the reference spectra, indicating that the peak height is not a good measure of the W valency. For reference spectra, however, there is a slight difference between W(V) and W(IV) at the lower-energy side of the white line; a shoulder structure appears in the W(V) reference (Cs salt) at $\sim$10196 eV, while it does not in the W(IV) ones (K salt). To clarify this finding, the first derivative spectra are also plotted in Fig. 4, and the shoulder structure clearly emerges. The spectra of sample (R3) $Co_2W^{IV}(CN)_8 \cdot zH_2O$ (not shown) are almost identical to those of the K salt. It is therefore concluded that pentavalent W can clearly be identified using this shoulder structure appearing at the lower-energy side of the white line.

Although the origin of the shoulder cannot be defined, it is reasonable to assign it to the singly occupied W $5d$ level that is present in the case of W(V). The local structure around W, which is discussed below in the EXAFS section, is $W(CN)_8Co_4$ (subscripts denote the coordination number) possibly with D_{2d} symmetry. Although it is not known which is the most stable orbital, $5d_{x^2-y^2}$ or $5d_{z^2}$, because of the lack of information on the bond angles, $5d$ electrons should occupy one of these orbitals. In the case of W(V), the lowest $5d$ orbital is singly occupied and the transition of W$2p \rightarrow 5d$ will be observed, while for W(IV), no transition will take place since the lowest $5d$ orbital is occupied by a pair of electrons. Another possibility of the origin of the transition is the exchange splitting where an unpaired electron is a singlet or a triplet coupled with an excited electron.

When we look at the spectra of samples (a) and (e) in Fig. 4, we find that a similar shoulder structure appears in the spectrum of sample (a) but not in that of sample (e). This clearly indicates that W is pentavalent in the HT phase and tetravalent in the LT one. Combining the above Co K-edge XANES results, we can conclude that at the spin transition, a Co $3d$ electron is transferred to W $5d$. The Co state is Co(II)HS ($d^7, S=3/2$) in the HT phase and Co(III)LS ($d^6, S=0$) in the LT phase, while the W electronic states are LS in both the HT and LT phases ($d^1, S=1/2$ and $d^2, S=0$, respectively). These results are consistent with the susceptibility measurements.[5]

C. W L_{III}- and Co K-edge EXAFS

EXAFS analysis was carried out in well-established procedures using the analysis code EXAFSH.[8] The EXAFS oscillation functions $k^3\chi(k)$ (k being the photoelectron wave number) were obtained by pre-edge base line subtraction, post-edge background estimation using cubic spline functions, and normalization with the atomic absorption coefficients.

Figures 5 and 6 show the W L_{III}-edge EXAFS functions $k^3\chi(k)$ and their Fourier transforms of samples (a)–(f), respectively. The employed Δk ranges in the Fourier trans-

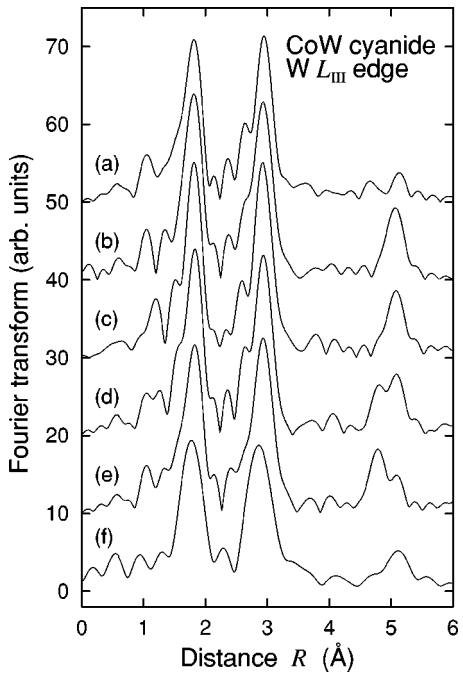

FIG. 6. Fourier transforms of Fig. 5. The employed Δk ranges in the Fourier transforms were around 3–16 ($Å^{-1}$), and were slightly dependent on the samples.

forms were approximately 3–16 $Å^{-1}$. Prior to the assignments of the Fourier peaks and subsequent curve-fitting analyses, we need to speculate the local structure of the present material. Figure 7 shows the expected local structure of CoW cyanide. W is coordinated by eight CN^- ligands, and Co is expected to show octahedral coordination. From elemental analysis, it was found that four NC^- and two 3-CNpy ligands are good candidates for the ligands of Co. The coordination of six NC^- is impossible from the elemental Co/W ratio, as long as W is surrounded by eight NC^-. Although H_2O coordination cannot be ruled out from the elemental analysis, the interaction with Co ions is much weaker than that of 3-CNpy. In 3-CNpy, coordination of the N atom on the aromatic ring is more likely because of the presence of lone-pair electrons. In the Fourier transforms of the W L_{III}-edge EXAFS functions, one can find three dominant contributions at ~1.9, ~2.9, and ~5.2 Å, which are attributed to the W-C, W-N, and W-Co shells, respectively. In sample (a), the W-Co shell is very weak due to the high

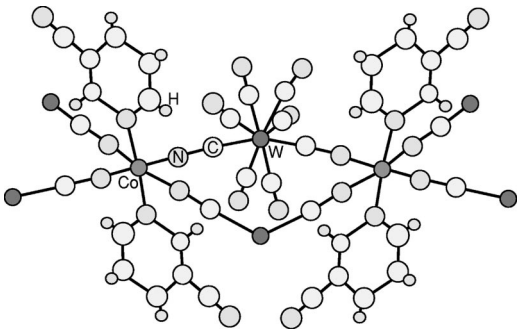

FIG. 7. Expected local structure of the CoW cyanide.

TABLE II. Results of EXAFS analysis of the W-C shell. Errors in parentheses correspond to those in the last digits. The fixed parameters in the curve fits were $S_0^2=0.91, N=8$, and $\Delta E_0=-0.4$ eV.

Sample	R(Å)	$C_2(10^{-2}$ Å$^2)$	R_f
(R1)	2.162(9)	0.19(7)	0.051
(R2)	2.160(10)	0.25(8)	0.081
(R3)	2.148(12)	0.17(13)	0.212
(a)	2.161(10)	0.28(10)	0.069
(b)	2.152(9)	0.20(8)	0.116
(c)	2.161(8)	0.18(8)	0.085
(d)	2.160(9)	0.20(9)	0.056
(e)	2.161(10)	0.25(9)	0.034
(f)	2.158(7)	0.23(8)	0.092

measurement temperature of 300 K. Because of the (nearly) linear configuration of the –W–C–N–Co– chain, the W-N and W-Co shells are noticeably enhanced due to the multiple-scattering focusing effect. The features of the W-C and W-N shells among spectra (a)–(f) do not differ so much from each other, indicating little structural change of the $W(CN)_8$ unit irrespective of the charge difference. On the other hand, the W-Co shell exhibits clear sample dependence, suggesting significant structural changes around Co.

In order to obtain structural information, curve-fitting analysis was performed in k space. For W L_{III}-edge EXAFS, the one-shell analysis can be adopted for the W-C and W-N shells, while the two-shell analysis is necessary for the W-Co shell since the W-Co(II) distance seems to be significantly different from the W-Co(III) one. Here we can employ the ratio of Co(II)/Co(III) obtained by the above factor analysis of Co K-edge XANES. Theoretical standards are evaluated using the FEFF6 code[9] assuming the $W(CN)_8Co_4$ cluster unit with appropriate interatomic distances R, edge-energy shifts ΔE_0, and Debye-Waller factors C_2. Here the $W(CN)_8$ unit was assumed to have cubic symmetry, although the actual structure should significantly be distorted. The backscattering amplitudes and the phase shifts for each shell [W-C, W-N, W-Co(II), and W-Co(III)] were extracted from the FEFF files and were used in the curve-fitting analysis. The ranges employed in the curve-fitting analysis were ΔR_{CF} ~1.35–2.10 Å and Δk_{CF}~4.0–14.0 $Å^{-1}$ for the W-C shell, ΔR_{CF}~2.45–3.35 Å and Δk_{CF}~4.0–14.0 $Å^{-1}$ for the W-N shell, and ΔR_{CF}~4.45–5.55 Å and Δk_{CF} ~6.0–16.0 $Å^{-1}$ for the W-Co shell (subscript ''CF'' means curve fit). The parameters of the intrinsic loss factor S_0^2, the coordination number N, and ΔE_0 were fixed throughout the curve-fitting analysis. R and C_2 were obtained as fitting variables. The obtained values of R and C_2 are tabulated in Tables II, III, and IV, together with the reliability factor R_f defined as

$$R_f=\sqrt{\frac{\Sigma_{i=1}^{N_d}[k_i^3\chi_{obs}(k_i)-k_i^3\chi_{calc}(k_i)]^2}{\Sigma_{i=1}^{N_d}[k_i^3\chi_{obs}(k_i)]^2}}, \qquad (1)$$

TABLE III. Results of EXAFS analysis of the W-N shells. R, C_2, and R_f are given. The fixed parameters in the curve fits were $S_0^2=0.91$, $N=8$, and $\Delta E_0=-1.2$ eV.

Sample	R(Å)	$C_2(10^{-2}$ Å$^2)$	R_f
(R1)	3.322(8)	0.26(7)	0.055
(R2)	3.318(11)	0.33(9)	0.045
(R3)	3.305(12)	0.35(10)	0.086
(a)	3.318(8)	0.33(8)	0.142
(b)	3.314(8)	0.30(6)	0.070
(c)	3.316(8)	0.30(7)	0.108
(d)	3.317(9)	0.30(8)	0.113
(e)	3.319(8)	0.30(7)	0.080
(f)	3.306(14)	0.35(15)	0.121

where N_d is the number of data.

The errors were estimated according to the IXS (International XAFS Society) report.[10] Several error estimation criteria have been proposed, but we will here employ the following scheme. The reliability factor χ_ν^2 is first defined as

$$\chi_\nu^2=\frac{N_p}{N_d(N_{ind}-N_p)}\sum_{i=1}^{N_d}\frac{[\chi_{obs}(k_i)-\chi_{calc}(k_i)]^2}{[\epsilon(k_i)]^2}, \quad (2)$$

where N_p and N_{ind} are the number of parameters and independent data points ($N_{ind}=2\Delta k_{CF}\Delta R_{CF}/\pi$), respectively. $\epsilon(k_i)$ is the error at each data point i, which was estimated from the signal-to-noise ratio of the experimental spectra. The upper or lower limit of the fitted variables was obtained so that

$$\Delta\chi_\nu^2=\chi_\nu^2-\chi_{\nu,opt}^2\leqslant 1, \quad (3)$$

where $\chi_{\nu,opt}^2$ is the optimized one. Note here that the errors obtained in Tables II–V include only the fitting one. No systematic errors derived from the fixed parameters of $N, \Delta E_0$, backscattering amplitudes, phase shifts, and so forth are included.

The W-C and W-N distances are found to be almost equal for all of the samples. In particular, it is noted that the W-C and W-N distances of the W(V) standard $Cs_3W^V(CN)_8$ are not different from those of $K_4W^{IV}(CN)_8$. Therefore, it is reasonable that all of the CoW cyanides show essentially the same W-C and W-N distances irrespective of the W valency. Such a similarity was also observed in our previous CoFe cyanide case,[2,3] the Fe-C and Fe-N distances do not vary with the change of the Fe valency. This can be explained as follows. The W $5d$ electrons participate in the π bonding with the CN^- ligands and the $5d$ electrons occupy the hybridized W$5d$-$CN^-2\pi^*$ bonding orbital. This implies that W(IV) can form stronger W-CN bonds than W(V) because of a greater number of $5d$ electrons. On the other hand, the ionic radius of W(IV) is larger than that of W(V). These two effects have compensated each other, resulting in almost equivalent W-C and W-N distances. In contrast, the W-Co(II) distance is noticeably different from the W-Co(III) one by as much as ~ 0.17 Å. This will be discussed after the analysis of Co K-edge EXAFS.

TABLE IV. Results of EXAFS analysis of the W-Co shell. R(Åunit), $C_2(10^{-2}$ Å^2 unit), and R_f are given. The fixed parameters in the curve fits were $S_0^2=0.91$, $N_{tot}=4$, and $\Delta E_0=-4.0$ eV. N_{tot} is the total coordination number of the W-Co^{II} and W-Co^{III} shells. For the Co^{II} ratio, the above XANES results in Table I were used.

Sample	W-Co^{II} R (Å)	W-Co^{II} C_2 $(10^{-2}$ Å$^2)$	W-Co^{III} R (Å)	W-Co^{III} C_2 $(10^{-2}$ Å$^2)$	R_f
(a)	5.35(2)	1.10(19)			0.176
(b)	5.37(1)	0.71(50)	5.22(6)	0.47(12)	0.134
(c)	5.36(2)	0.42(14)	5.20(4)	0.42(31)	0.146
(d)	5.36(2)	0.34(17)	5.18(3)	0.55(25)	0.109
(e)	5.36(3)	0.33(24)	5.18(2)	0.49(16)	0.098
(f)	5.38(2)	0.37(13)	5.24(7)	0.43(58)	0.070

TABLE V. Results of EXAFS analysis of the Co-N shell. R, C_2, and R_f are given. The parameters fixed in the curve fits were $S_0^2=1.00$, $N_{tot}=6$ and $\Delta E_0=-5.0$ eV. N_{tot} is the total coordination number of the Co^{II}-N and Co^{III}- N shells. For the Co^{II} ratio, above XANES results in Table I were used.

Sample	Co^{II}-N R (Å)	Co^{II}-N C_2 $(10^{-2}$ Å$^2)$	Co^{III}-N R (Å)	Co^{III}-N C_2 $(10^{-2}$ Å$^2)$	R_f
(a)	2.072(13)	0.74(18)			0.161
(b)	2.072(12)	0.86(17)			0.209
(c)	2.087(12)	0.55(22)	1.904(24)	0.37(23)	0.141
(d)	2.086(15)	0.45(22)	1.899(15)	0.36(22)	0.243
(e)	2.117(25)	0.53(25)	1.911(13)	0.36(16)	0.195

Figures 8 and 9 show the Co K-edge EXAFS functions $k^3\chi(k)$ and their Fourier transforms of samples (a)–(e), respectively. At high-k regions above ~ 11 Å^{-1}, quite intense short-period oscillations are found, which originate from the Co-W contribution. In Fig. 9, several complicated peaks are observed; those in the range of approximately 1–2 Å and 4.3–5.4 Å are ascribed to the Co-N and Co-W shells, respectively. These features are significantly dependent on the samples, indicating noticeable structural difference around Co between the HT and LT phases. The features appearing in the 2–4 Å range are more complicated; there should exist contributions not only from the C atoms of the NC^- ligands but also from the C atoms of the 3-CNpy molecules.

A curve-fitting analysis for Co K-edge EXAFS was performed in a similar manner, though it was more complicated. First, simulation of the EXAFS function was attempted by using FEFF6.[9] Employing a cluster consisting of $Co(NC)_4(3\text{-}CNpy)_2W_4$ with appropriate distances, FEFF6 calculations were performed. We simulated the Co(II) and Co(III) cases separately and subsequently added them using the above-determined Co(II)/Co(III) ratio for comparison with experimental spectra. The calculated results are depicted also in Figs. 8 and 9 for sample (b). Agreement between the experimental spectrum and the simulation is fairly good in spite of the fact that the interatomic distances or the

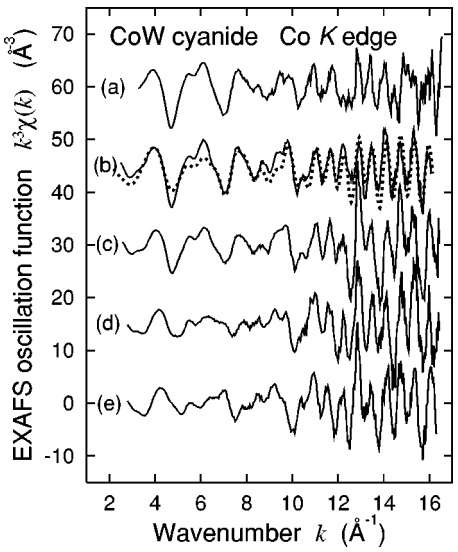

FIG. 8. Co K-edge EXAFS oscillation functions $k^3\chi(k)$ of samples (a)–(e) (solid lines), together with the simulated result using FEFF6 for sample (b) (dotted lines). Note that fitting variables such as R and C_2 are not optimized. The temperatures of the measurements are 300 K for sample (a), 30 K for samples (b)–(d), and 130 K for sample (e).

Debye-Waller factors are not optimized. Although it is difficult to eliminate other possibilities for the local structure around Co, the present model shown in Fig. 7 may be the best candidate both from the chemical and EXAFS points of view. For instance, if Co were coordinated by the NC ligand of CNpy, the Co-C contribution around 2–3.5 Å in Fig. 9 would be as intense as the Co-N one, as in the case of W L_{III}-edge EXAFS.

A curve-fitting analysis for the Co-N and Co-W shells was subsequently performed in k space. Here the two-shell analysis was basically employed since the Co(II)-N and Co(III)-N distances are considerably different from each other. The employed ranges are $\Delta R_{CF}\sim 1.05$–2.00 Å and $\Delta k_{CF}\sim 4.0$–14.0 Å^{-1} for the Co-N shell and $\Delta R_{CF}\sim 4.35$–5.60 Å and $\Delta k_{CF}\sim 4.0$–14.0 Å^{-1} for the Co-W shell. The parameters of S_0^2, N, and ΔE_0 were fixed throughout the analysis; $S_0^2=1.00$ for all of the shells, $N_{tot}=6$ and $\Delta E_0=-5.0$ eV for the Co-N shell, $N_{tot}=1.5$ for the W-Co shell, $\Delta E_0=-5.0$ eV for the W-Co(II) shell, and $\Delta E_0=0.0$ eV for the W-Co(III) shell. The ratios of Co(II)/Co(III) were estimated from the above Co K-edge XANES analysis. R and C_2 were obtained as fitting variables. The obtained structural parameters are tabulated in Tables V and VI. The errors were estimated in a manner similar to above. Although some contributions in the 2–3.5 Å range can be observed in Fig. 9, we have given up the analysis since too many possible shells of the C atoms in NC^- and pyridine are overlapped.

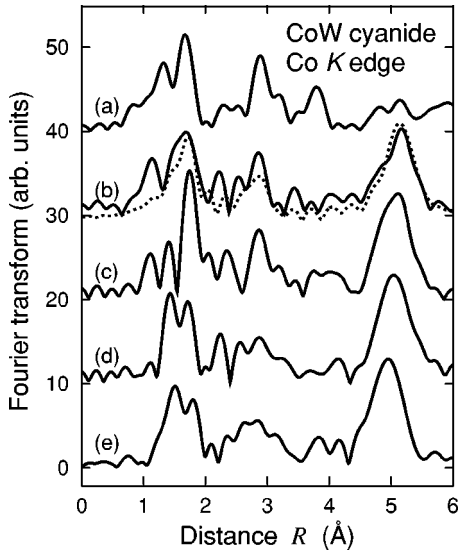

FIG. 9. Fourier transforms of Fig. 8. The employed Δk ranges in the Fourier transforms were around 3–16 (Å^{-1}) and were slightly dependent on the samples.

TABLE VI. Results of EXAFS analysis of the Co-W shell. R, C_2, and R_f are given. The parameters fixed in the curve fits were $S_0^2=1.00$, $N_{tot}=1.5$, and $\Delta E_0=-5.0$ eV [W-Co]$^{\mathrm{II}}$ or 0.0 eV [W-Co]$^{\mathrm{III}}$. N_{tot} is the total coordination number of the Co$^{\mathrm{II}}$-W and Co$^{\mathrm{III}}$-W shells. For the Co$^{\mathrm{II}}$ ratio, above XANES results in Table I were used.

Sample	Co$^{\mathrm{II}}$-W R (Å)	Co$^{\mathrm{II}}$-W C_2 (10^{-2} Å^2)	Co$^{\mathrm{III}}$-W R (Å)	Co$^{\mathrm{III}}$-W C_2 (10^{-2} Å^2)	R_f
(b)	5.37(1)	0.71(50)	5.22(6)	0.47(12)	0.123
(c)	5.37(2)	0.23(12)	5.14(3)	0.20(21)	0.110
(d)	5.37(3)	0.20(18)	5.15(2)	0.25(16)	0.109
(e)	5.43(6)	0.32(41)	5.16(1)	0.17(8)	0.098

In Tables V and VI, it is clear that the Co(II)-N distance is noticeably different from the Co(III)-N one by as much as ~0.17 Å. Correspondingly, the Co(II)-W and Co(III)-W distances deviates from each other. Comparing the results with those in Table IV, the W-Co(II) distance (5.37 ±0.02 Å) is consistent with the Co(II)-W one (~5.36 ±0.02 Å), indicating reliable estimation of the distance between Co(II) and W. The Co(III)-W distance (5.15 ±0.02 Å) is also in accordance with the W-Co(III) one (5.19±0.02 Å) within the error range, although the deviation is a little larger.

Judging from the distances obtained in Tables I–VI, the alignment of –W–C–N–Co– is confirmed to be almost linear as in the case of rocksalt-type Prussian blue analogs such as CoFe cyanides.[2,3] This is reasonable because of the π bonding nature between metal cations and CN^- ligands.

IV. CONCLUSIONS

We have investigated W L- and Co K-edge XAFS of CoW cyanide. Co K-edge XANES has clarified that the HT phase consists of Co(II)HS and the LT one of Co(III)LS. We have also determined quantitatively the Co(II)/Co(III) composition ratios by means of factor analysis. W $L_{\mathrm{III,II}}$-edge XANES has revealed that the W valency is pentavalent in the

HT phase, while it is tetravalent in the LT phase. This conclusion is based on the finding of the shoulder structure at the lower-energy side of the white line in the case of pentavalent W. Upon spin transition, the Co $3d$ electron is transferred to W $5d$, and this is associated with the electronic configuration change from Co(II)HS($S=3/2$)-W(V)($S=1/2$) to Co(III)LS($S=0$)-W(IV)($S=0$). The HT phase is formed not only by heating the LT phase at ~ 200 K but also by irradiation of x rays at 30 K. Moreover, rapid cooling of the HT phase allows the material to stay at the trapped HT phase even at very low temperatures.

The local structure around W and Co atoms has been determined by W L_{III}- and Co K-edge EXAFS. The model structure is schematically shown in Fig. 7. Although little structural changes are observed in the $W(CN)_8$ unit on the spin transition, the Co-N distances are noticeably decreased by as much as ~ 0.17 Å from the HT phase to the LT phase. The –Co–N–C–W– configuration is found to be almost linear. Since the structural change is quite drastic, the trapped HT phase is very stable at low temperature.

ACKNOWLEDGMENTS

The authors are grateful for the Grant-in-Aid for Scientific Research (No. 10304059) from the Ministry of Education, Culture, Sports, Science, and Technology. The present work has been performed under the approval of the Photon Factory Program Advisory Committee (PF-PAC No. 2000G071).

*Electronic address: toshi@chem.s.u-tokyo.ac.jp; http://www.chem.s.u-tokyo.ac.jp/~ssphys/toshi/toshiE.html

[1] O. Sato, T. Iyoda, A. Fujishima, and K. Hashimoto, Science **272**, 704 (1996).

[2] T. Yokoyama, T. Ohta, O. Sato, and K. Hashimoto, Phys. Rev. B **58**, 8257 (1998).

[3] T. Yokoyama, M. Kiguchi, T. Ohta, O. Sato, Y. Einaga, and K. Hashimoto, Phys. Rev. B **60**, 9340 (1999).

[4] C. Cartier dit Moulin, F. Villain, A. Bleuzen, M.A. Arrio, P. Sainctavit, C. Lomenech, V. Escax, F. Baudelet, E. Dartyge, J.J. Gallet, and M. Verdaguer, J. Phys. Chem. **122**, 6653 (2000).

[5] K. Hashimoto *et al.* (unpublished).

[6] A. Bianconi, M. Dell'Ariccia, A. Gargano, and C. R. Natoli, *EXAFS and Near Edge Structure, Springer Series in Chemical Physics* Vol. 27, edited by A. Bianconi, L. Incoccia, and S. Stipcich (Springer, Berlin, 1983), p. 57.

[7] M. Fernández-García, C. Márquez Alvarez, and G.L. Haller, J. Phys. Chem. **99**, 12 565 (1995).

[8] http://www.chem.s.u-tokyo.ac.jp/~ssphys/toshi/soft/ soft.html; T. Yokoyama, H. Hamamatsu, and T. Ohta, computer code EXAFSH, version 2.1, The University of Tokyo, 1993.

[9] S.I. Zabinsky, J.J. Rehr, A. Ankudinov, R.C. Albers, and M.J. Eller, Phys. Rev. B **52**, 2995 (1995).

[10] http://ixs.iit.edu/survey/errors/